Roles of Nanofiber Scaffold Structure and Chemistry in Directing Human Bone Marrow Stromal Cell Response

Abstract

Nanofiber technology has emerged as a promising tool to recapitulate native extracellular matrix structure; however the properties of nanofibers governing cell-material interactions are still largely undetermined. We have investigated the role of both nanofiber structure and chemistry in directing the response of human bone marrow stromal cells (hBMSCs). We developed a poly(ε-caprolactone) (PCL) nanofiber material system where scaffold structure is maintained while surface chemistry is modified via mild sodium hydroxide (NaOH) hydrolysis to introduce surface carboxyl groups. Surface carboxyl groups were verified via x-ray photoelectron spectroscopy (XPS), water contact angle (WCA), and toluidine blue-O biochemical assay and scaffold structure was verified with scanning electron microscopy (SEM). hBMSC response was investigated for proliferation, differentiation (alkaline phosphatase activity and mineralization), cell morphology,and microarray gene expression profiles. We found that both nanofiber structure and chemistry play a role in hBMSC osteogenic differentiation where PCL nanofiber scaffolds were able to elicit an osteogenic phenotype, while chemically modified PCL nanofiber scaffolds did not. Scaffold structure was found to have a more dominant effect on cell morphology and extracellular matrix gene expression while nanofiber chemistry had a larger effect on genes related to metabolism and cytoskeletal rearrangement. The nanofiber scaffold material system developed here can serve as a platform to further investigate the role of microenvironmental cues on osteogenic differentiation. The NaOH modified NF scaffolds are particularly useful as a negative control for osteogenic differentiation in NF scaffolds.

Keywords: Nanofiber scaffold; Stem cells; Surface modification; Bone tissue engineering; Microarray gene expression; Cell morphology

Research Article

Volume 1 Issue 1 - 2016

SarkarS[1]*, Baker BA[1], ChenD[2], Pine PS[1], McDaniel JH[1], Salit ML[1], LosertW[2], Simon CG[1] and DunkersJ[1]

[1]*Biosystems and Biomaterials Division,National Institute of Standards & Technology, USA*

[2]*Department of Physics, University of Maryland, USA*

***Corresponding author:** Sumona Sarkar, National Institute of Standards and Technology, 100 Bureau Dr, Gaithersburg,MD20899,USA,Tel: (301)-975-8595; Fax: 301-975-4977; Email: sumona.sarkar@nist.gov

Received: July 14, 2016 | **Published:** August 22, 2016

Abbreviations: ECM: Extracellular Matrix; COOH: Carboxyl Functionality; NH_2: Amine functionality; OH: Hydroxyl Functionality; hBMSC: Human Bone Marrow Stromal Cell; NF: PCL Non-Woven Nanofibers; TCPS: Tissue Culture Polystyrene; SEM: Scanning Electron Microscopy; SC films: PCL Spin-Coated TCPS discs; NaOH: Sodium Hydroxide; DI: De Ionized; MOD NF: NF Scaffolds Modified By Mild Hydrolysis; MOD SC: SC Films Modified by Mild Hydrolysis; TBO: Toluidine Blue-O; XPS: X-ray Photoelectron Spectroscopy; At %: Atomic Concentrations; CO_2: Carbon Dioxide; EDTA: EthyleneDiamine Tetra Actate; OS: Osteogenic Supplement; PBS: Phosphate Buffered Salt Solution; DNA: Deoxyribonucleic Acid; ALP: Alkaline Phosphatase; AR: Alizarin Red; BSA: Bovine Serum Albumin; NA: Numerical Aperture; RNA: Ribonucleic Acid; NIST: National Institute of Standards and Technology; ERCC: External RNA Controls Consortium; SAM: Significance Analysis of Microarrays; ALL NF: NF and MOD NF; ALL SC: SC and MOD SC; ALL UN-MOD: NF and SC; GO: Gene Ontology; KEGG: Kyoto Encyclopedia of Genes and Genomes; DAVID: Database for Annotation Visualization and Integrated Discovery; WCA: Water Contact Angle; C_v: Coefficient of Variation; MC3T3-E1: Osteoblast-like cells; ALPL: Gene for Alkaline Phosphatase; COL8A2: Gene for Collagen Type VIII Alpha 2; FNDC1: Gene for Fibronectin Type III Domain Containing 1,FBLN5: Gene for Fibulin 5; GPC4: Gene for Glypican 4; IGFBP1: Gene for Insulin Like Growth Factor Binding Protein 1; IGF: Insulin Like Growth Factor; IL 8: Gene For Interleukin 8; KRT18: Gene for Keratin 18; RHOA: Gene Forras Homolog Gene Family; TUBB6: Gene for Tubulin; TUBBP1: Gene for Similar to Tubulin; *E. coli*: *Escherichia coli*; PFKFB4: Gene for 6-Phosphofructo-2-Kinase/Fructose-2,6-Biphosphatase 4; TPI1: Gene for Triosephosphate Isomerase 1; ENO2: Gene for Enolase 2; PCK2: Gene for PhosphoenolpyruvateCarboxykinase 2; PFKP: Gene for Phosphofructokinase

Introduction

Nanofiber technology has emerged as a promising tool to recapitulate the native extracellular matrix (ECM) environment for tissue engineering and regenerative medicine strategies [1-3]. A wide range of fibrous scaffolds have been fabricated from both natural and synthetic polymers with control over fiber diameter, alignment, chemical and biological functionalization, and scaffold properties [3-5]. Nanofiber materials have been demonstrated to promote desirable cell-material interactions that affect properties such as cell attachment, morphology, differentiation, protein adsorption and ECM deposition [3].

Structural cues in the nanofiber environment are often attributed to these effects and are largely dependent on the

nanofiber mat properties such as fiber diameter, alignment and porosity [4,6-8]. Biological functionalization and chemical modification have also been demonstrated have significant effects on NF scaffolds. For example, Chua et al. [7] functionalized the surface of polyethersulfonenanofibers and investigated the effects of carboxyl (-COOH), amine ($-NH_2$) and hydroxyl (-OH) functionalities on hematopoietic stem/progenitor cell culture expansion [7]. They found that amine functionalized nanofibers supported the highest degree of cell adhesion and expansion however the mechanisms behind this enhanced functionality are largely undetermined [7]. In order to better understand the mechanisms underlying cell-material interactions in the nanofiber environment, systematic studies with controlled material properties and culture conditions are required.

Several studies have demonstrated the strong potential for the use of nanofiber scaffolds in bone tissue engineering, where osteogenic differentiation is enhanced on nanofiber scaffolds [9-13]. In a recent study conducted by Kumar et al. [14], the importance of the nanofiber scaffold structure in directing stem cell fate down an osteogenic linage was further supported. The study isolated the effect of scaffold structural cues in the direction of stem cell fate by systematically investigating scaffolds of similar chemical compositions with varying 3D architectures. Surprisingly, only nanofiber scaffolds were able to promote human bone marrow stromal cell (hBMSC) osteogenic differentiation in the absence of osteogenic differentiation supplements [14]. Cells on these materials also had elongated branched morphologies and cytoskeletal gene expression profiles consistent with those cells cultured in the presence of osteogenic supplement, supporting possible cell morphology based mechanisms behind stem-cell nanofiber interactions [14]. In the current study, we further investigate the role of cell morphology in the osteogenic response of stem cells to nanofiber scaffolds.

To investigate the contributions of both nanofiber structure and surface chemistry in directing stem cell response and osteogenic differentiation, we have developed a material system with nanofiber scaffolds of similar structure but significantly different chemistry. Methods are available to tune and modify the surface chemistry of nanofibers [8,15-17]. However, surface modification of the nanofibers can be destructive to the nanofiber morphology. This is especially apparent in plasma oxidation of nanofiber scaffolds [16,18]. To minimize physical variability in nanofiber mat structure while changing fiber chemistry, we have utilized the wet chemical surface modification technique of base hydrolysis [8,11,15,19-21] to minimally effect scaffold structure while significantly altering scaffold surface chemistry. hBMSC proliferation, osteogenic differentiation, morphology, and microarray gene expression were then investigated on this material system as a function of scaffold structure and chemistry to better understand the contributions of these properties on stem cell response to nanofiber materials.

Materials and Methods

Certain commercial equipment, instruments, or materials are identified in this paper in order to specify the experimental procedure adequately. Such identification is not intended to imply recommendation or endorsement by the National Institute of Standards and Technology, nor is it intended to imply that the materials or equipment identified are necessarily the best available for the purpose.

Electrospun nanofiber mat fabrication

Nanofibers were fabricated from poly(ε-caprolactone) (PCL, relative molecular mass 80,000 g/mL, Sigma) using a custom-built electrospinning apparatus [14]. Electrospinning parameters such as solvent composition (3:1-9:1 volume ratio of chloroform: methanol), flow rate (0.5 mL/h and 2 mL/h), and PCL concentration (0.1 g/mL and 0.15 g/mL) were systematically varied (data not shown) to obtain fibers of approximately 600 nm diameter with low fiber diameter variability (Coefficient of variation (C_v) of 0.14). PCL solution was prepared in a 5:1 volume ratio chloroform: methanol solution at a 0.15 g/mL PCL concentration. The polymer solution was loaded into a 3 mL syringe and dispensed with a syringe pump at 0.5 mL/h through a 21 gauge 1" shaft, flat tip, dispensing needle. The positive lead from a power supply was affixed to the needle while the ground lead was fixed to the target (aluminum foil collection plate). The distance between the needle and target was approximately 21 cm and the voltage applied was 13 kV. Non-woven PCL nanofibers (NF) were collected onto approximately 0.95 cm diameter hot punched tissue culture polystyrene (TCPS) discs for 6 h (3 mL of solution dispensed). NFs collected on TCPS discs were removed from the foil target and assessed for morphology with scanning electron microscopy (SEM), chemical characterization, or adhered to the bottom of 48-well plates using silicone grease (Dupont) for cell culture experiments.

2D spin coated PCL films

PCL coated surfaces were prepared by spin-coating PCL solution (0.7 mL, 0.1 g/mL PCL in glacial acetic acid) at 104.72 rad/s (1000 rpm) for 20 s onto a TCPS dish (100 mm diameter). Films were air dried at room temperature overnight then heated above 60°C repeatedly to adhere the PCL to the TCPS surface as well as achieve a characteristic and repeatable cobblestone pattern. PCL coated TCPS discs (SC films) 0.95 cm in diameter were then hot punched from the TCPS dish. SC films were prepared for SEM imaging and chemical characterization or adhered to the bottom of 48-well plates for cell culture. These SC films served as a control 2-D analogues to the NF scaffolds.

Scaffold Sterilization

NF scaffolds and SC films were secured in 48-well plates with silicone grease. Plates were then sterilized by ethylene oxide treatment (12 h cycle, 48 h degassing under house vacuum). All subsequent handling was carried out in sterile conditions.

Scaffold chemical modification

NF scaffolds and SC films were treated via mild hydrolysis in sodium hydroxide (NaOH) solution in order to expose carboxyl (COOH) and hydroxyl (OH) groups on the material surface and render scaffolds more hydrophilic (Figure1)[15,19]. Scaffold hydrolysis was tuned to maximize surface COOH concentration while minimizing structural changes. Parameters including NaOH concentration (0.1 mol/L to 5 mol/L), incubation time (1 h to7 h), and incubation temperature (25°C and 37°C) were systematically varied (Data not shown). In a final procedure, scaffolds were

hydrolyzed in freshly prepared 1 mol/L sodium hydroxide (NaOH) solution in sterile filtered deionized (DI) water. Briefly, 500 µL of 1 mol/L NaOH solution was pipetted onto the scaffolds (500 µL of DI water was used for the un-modified case) and incubated at 37°C under constant agitation for 7 h. Scaffolds were then rinsed 2x with sterile DI water followed by a 30 min rinse in DI water under constant agitation. Scaffolds were rinsed again 2x with sterile DI water, then set in a sterile cell culture hood overnight to dry. NF scaffolds and SC films modified by mild hydrolysis are denoted as MOD NF and MOD SC respectively. Modified scaffolds were tested immediately for surface chemical properties or immediately immersed in cell culture medium containing fetal bovine serum, in preparation for cell seeding.

Scanning electron microscopy (SEM)

NF and MOD NF scaffold and SC and MOD SC film morphology were investigated using SEM. Substrates were sputter coated with gold (90 s, 15 mA) then imaged on a Hitachi S-4700-II FE-SEM at 5 kV (5000 X and 50,000 X magnification). Fiber diameter was determined from scanning electron micrographs from five fields of view using ImageJ software (National Institute of Health) to determine average fiber diameter and fiber diameter variability (> 80 fibers investigated per group) before and after chemical modification.

Contact angle goniometry

Surface wettability was investigated via water contact angle goniometery. DI Water droplets (approximately 100 µL) were dispensed onto the scaffold and film surfaces, imaged and modeled using sessile drop fitting to obtain contact angle measurement (averaged across 4 samples, 3 spots per sample).

Toluidine Blue-O assay for carboxyl functional groups

Carboxyl concentration was determined using the toluidine blue-O (TBO) reagent [22-26]. Substrates were soaked in 1 ml of 0. 5 mmol/L TBO (buffered to pH 10 at room temperature) for 5 h under constant agitation. Non-complexed dye was then removed by rinsing in an excess of 0. 1 mmol/L NaOH. Complexed dye was then desorbed from the surface by incubating each substrate in 500 µL of 500 mL/L glacial acetic acid solution in DI for 10 min under vortexing. Desorbed dye solution was then plated into a 96-well plate (200 µL per well) and the absorbance was measured at 633 nm wavelength. A calibration curve of TBO solutions of known TBO concentration was generated to determine the concentration of carboxyl groups on the scaffold or film surface [24,25]. The surface density of carboxyl groups was calculated under the assumption that the TBO complexes to equivalent moles of carboxyl groups on the surface (a 1:1 carboxyl: TBO relationship)[22,23].

X-ray photoelectronspectroscopy (XPS)

XPS was used to conduct an elemental analysis of the NF, MOD NF, SC and MOD SC surfaces. Spectra were obtained on a Kratos AXIS Ultra DLD spectrometer with a monochromatic Al x-ray source (1486.7eV) operating at 140 W under approximately 1.0 x 10^{-9}Torr (1.33 x 10^{-11} Pa) vacuum (Supplemental Information M1). Atomic concentrations (At %) were calculated from survey spectra. Three spectra were acquired for each sample, and triplicate samples were investigated for each group.

Human bone marrow stromal cell (hBMSC) culture

Sterile TCPS discs, NF scaffolds, MOD NF scaffolds, SC films, and MOD SC films secured in 48-well plates were soaked in culture medium (α-minimum essential medium (*Invitro*gen) supplemented with 165 mL/L fetal bovine serum (FBS, Atlanta Biologics), 4 mmol/L ι-glutamine and 10 mL/L Penicillin/ Streptomycin (Cellgro)) for 48 h to facilitate protein deposition. Primary human bone marrow stromal cells (hBMSCs, from 24 year old Female, Tulane Center for Gene Therapy) were cultured at 37°C with 5 % by volume CO_2 in culture medium. For cell seeding, hBMSCs were allowed to achieve 80% confluence in a T-75 culture flask before dissociation with 0.25 % mass fraction trypsin (containing 1 mmol/L ethylenediaminetetraactate (EDTA)) and re-suspended in culture medium. Cell number was determined using a hemocytometer. Passage 5 cells were seeded onto scaffolds in 48-well plates at 10,000 cells/cm^2(scaffolds for cell imaging and alkaline phosphatase activity assay were seeded at 5,000 cells/cm^2). Cells were seeded in 500 µL of cell suspension in culture medium per well. Positive control TCPS + osteogenic supplement (OS) cultures were supplemented with 10 nmol/L dexamethasone, 20 mmol/L β-glycerophosphate and 0. 05 mmol/L ascorbic acid. Medium was changed twice per week with culture medium or culture medium supplemented with OS. Cells were cultured to 1 d, 4 d, 14 d, and 50 d as indicated.

Picogreen DNA assay

The Picogreen DNA assay was used to assess cell proliferation by measuring DNA concentration. At 1 d and 14 d time points, samples (including no cell controls) were rinsed with PBS then frozen overnight at -20°C to rupture cell membranes. Cultures were then digested for 16 h at 60°C in digestion buffer (0.1 mL papain solution (activity 35 U/mg) and 35 mg cysteine in 20 mL PBS). Cell lysate solution was then transferred to a 96-well plate and diluted 1:1 in Picogreen reagent (Invitrogen, 200 µL). DNA fluorescence (excitation 485 nm, emission 515 nm) was measured using a platereader and calibrated using a DNA standard curve.

Alkaline phosphatase assay

Alkaline phosphatase (ALP) concentration was detected using the Stanbio alkaline phosphatase assay kit according to kit procedures. ALP was measured at 4 d and 14 d time points. Briefly, samples and controls (TCPS and TCPS+OS) were rinsed with PBS (37°C). Cells were then lysed by incubating in 10mL/L NP-40 detergent (Stanbio) in DI water for 10 min at 37°C. 50 µL of cell lysate was assayed using the p-Nitrophenylphosphate(17. 0 mmol/L) reaction solution in 24-well plates. NP-40 solution with reagent was used as a blank and an ALP standard curve was generated from freshly reconstituted control sera with known alkaline phosphatase levels (Normal Control Serum, StanbioSer-T-Fy 1). Absorbance values were read on a platereader at 405 nm every 20 min for 5 h. Change in normalized absorbance per minute was calculated from a linear region of the curve and used to calculate units per liter of ALP. ALP concentration was then normalized to DNA concentration from parallel cultures (Picogreen DNA assay).

Alizarin red (AR) staining for mineral deposition

Cultures were fixed in 37 g/L formaldehyde in phosphate buffered saline (PBS, 37°C) for 20 min, rinsed with DI water then

stained (1 h) for mineral deposition with Alizarin red solution (0.5 mg/mL in DI water). Samples were rinsed extensively with DI water to remove excess stain (rinse was considered complete when paired control samples with no cells did not show distinct staining patterns). Digital images (5X magnification) of stained samples were acquired using a stereomicroscope. Four samples from each treatment group were imaged for their mineral deposition.

Confocal fluorescence imaging of cells and cell shape analysis

Confocal microscopy (Leica SP5) was used to characterize cell morphology of hBMSCs cultured for 1 d on NF, MOD NF, SC and MOD SC samples (cell seeding density, 5,000 cells/cm^2). Cells were fixed in 37 g/L formaldehyde in phosphate buffered saline (PBS, 37°C) for 1 h, rinsed with fresh PBS, then permeablized with 1 g/L Triton X-100 solution for 10 min. Samples were then rinsed with blocking buffer (50 g/L bovine serum albumin (BSA)) for 30 min. Actin cytoskeleton was fluorescently labeled with Alexa Fluor 546-phalloidin (0.33 µmol/L in blocking buffer, incubated for 30 min) while the nucleus was stained with DAPI (4',6-Diamidino-2-Phenylindole, Dihydrochloride) fluorescent stain (0.03 mmol/L in 10 g/L BSA, incubated for 5 min). Samples were rinsed in PBS before imaging. High resolution z-stack images were captured with a 63 x/0.90 numerical aperture (NA) water immersion objective (1024 x 1024 resolution, 1 µm z-step size). High-resolution confocal z-stack images of cells were necessary in order to capture fine feature of the cell boundary and also to capture cell processes that penetrate the porous NF scaffold. Only cells with no cell-cell contacts were analyzed to clearly delineate individual cell shape. Three samples were prepared for each treatment and over 35 cells were imaged and analyzed for each sample type.

Cell outlines were obtained by implementing a modified snake algorithm [27] as previously described by Driscoll et al. [28,29] (Supplemental Information M2) A total of 10 shape descriptors were calculated including cell area (µm^2), perimeter (µm), mean boundary distance (µm), major axis length (µm), mean negative curvature (1/µm), regions of negative curvature (normalized to perimeter), tortuosity, circularity, solidity, aspect ratio. For a description of cell shape metrics, (SupplementaryTable S1).

Human genome microarray

Total RNA from hBMSCs cultures were collected at 14 d (Supplemental Information M3). Whole genome transcriptions of hBMSCs were measured by high-throughput microarray screening using the Illumina HumanHT-12 v4 Expression BeadChips(IL1-HTH-110) with 47,231 probes through a contract with Expression Analysis Inc. (Durham, NC). Prior to microarray screening NIST ERCC spike-in controls were added to samples to monitor the quality of microarray data acquisition.

Microarray data was analyzed using the BRB-ArrayTools developed by Dr. Richard Simon and the BRB ArrayTools Development Team (version 4.1.0, Biometric Research Branch, National Cancer Institute) (Supplemental Information M4). From a total of 47,231 genes identified with the microarray, a subset of 199 genes was found to exhibit at least a 1.5-fold change from the median value of each gene (Figure 7a). The "significance analysis of microarrays" (SAM) [30] method was used to identify differentially expressed genes across class comparisons. Scaffolds were grouped into classes of ALL NF (NF and MOD NF), ALL SC (SC and MOD SC), ALL MOD (MOD NF and MOD SC), and ALL UN-MOD (NF and SC) for investigation of the effects of structure and chemistry on gene expression. Differentially expressed genes from SAM analysis were used for further gene ontology-based (GO) annotation in the Database for Annotation, Visualization, and Integrated Discovery (DAVID) [31,32] (Supplemental Information M4).

Average fold change values for select individual genes were calculated based on their $\log_2$ fold changefrom the average TCPS control value for that gene (Supplemental Information M5).

Results

Chemistry of scaffolds modified via mild hydrolysis

Water contact angle (WCA) dropped significantly with mild hydrolysis treatment on both NF scaffolds and SC films (from 145°±6°to 112°±4° on NF to MOD NF and 75°±7° to 48°±7°on SC to MOD SC) (Figure 2A). It should be noted however that contact angle measurements on nanofiber surfaces cannot provide a quantitative measure of surface energy due to the porous and irregular nature of the fiber mat surface [35]. A corresponding increase in COOH concentration was also detected on NF scaffolds where COOH concentration increased from 1.6 µmol/L ±1.1 µmol/L on NF scaffolds to 6. 6 µmol/L ± 1.1 µmol/L on MOD NF scaffolds (Figure 2A). No significant increase in COOH concentration was detected on MOD SC films compared to SC film. Elemental survey scans of the scaffold surfaces via XPS detected an increase in O 1s on MOD NF scaffolds compared to NF scaffolds attributable to opening of carboxyl groups and hydroxyl groups on the MOD NF scaffold surface (Figure 2B)[19]. In addition, Na 1s was detected on MOD NF scaffolds and MOD SC films. The overall O 1s to C 1s ratio was increased significantly on MOD NF scaffolds compared to NF scaffolds (Figure 2C). There was no significantly detected increase on O 1s species on MOD SC films compared to SC films. It can be assumed however, based on the mechanisms of base hydrolysis as well as the significant decrease in water contact angle on modified SC films, that carboxyl and hydroxyl groups were generated at physically significant concentrations on the SC film material surface. (Supplemental Information R1).

Structure of NaOH modified scaffolds

SEM images demonstrate the similarities between overall NF scaffold structure between NF scaffolds and MOD NF scaffolds, and maintenance of individual nanofiber morphology (Figure 3A). In MOD NF scaffolds, there is no evidence of fiber pitting or breakage typically seen with alkaline hydrolysis of PCL (Supplementary Figure S1). Mean fiber Diameter and fiber diameter variability (represented by the coefficient of variation, C_v) were quantified from SEM images (magnification 5000) (Figure 3B). Average nanofiber diameter for NF and MOD NF scaffolds was 611 µm and 600 µm respectively with C_v of 0.142 and 0.169 respectively. Mean fiber diameter and variance in fiber diameter between NF

and MOD NF scaffolds were not found to be statistically different (Figure3B). SC Films were also chemically modified by NaOH hydrolysis to alter surface chemistry while maintaining the overall film structure. SC films were imaged at magnification 1000 and magnification 50,000 to monitor the film structure with NaOH hydrolysis (Figure 3A). Films maintained their characteristic cobble stone pattern seen before and after chemical modification.

Effect of scaffold structure and chemistry on hBMSC proliferation

No significant differences in DNA concentration were seen after one day of culture (Figure 4). After 14 d of culture DNA concentration increased compared to Day 1 for all scaffolds, indicating that hBMSCs attached and proliferated on all scaffolds investigated. At 14 d of culture, there were no significant differences between DNA concentration on NF versus MOD NF or SC versus MOD SC, indicating that presence of -COOH/-OH groups on the scaffold surface had no effect on hBMSC proliferation (Figure 4). There was however a trend of increased cell proliferation on SC films compared to NF scaffolds, with MOD SC films having significantly higher DNA concentration than MOD NF films (Figure 4). Keselowsky et al. [39] saw similar results when investigating osteoblast-like cells (MC3T3-E1) on self-assembled monolayers of -OH, -COOH, -CH_3, and -NH chemistries, where no significant differences in cell proliferation were observed with varying surface chemistry [39]. This is a particularly important outcome, as it allows the comparison of other biological outcomes which may be influenced by cell viability and proliferation (i. e. mineralization and differentiation assays).

Differentiation of hBMSCs on chemically modified scaffolds

Alkaline phosphatase (ALP) is a metalloenzyme implicated in the early stages of mineralization and often used as a biomarker for osteogenic differentiation [40,41]. ALP activity was significantly higher in TCPS+OS controls at 4 d compared to all other substrates (Figure 5A). At 14 d ALP activity on NF scaffolds was significantly higher than on SC films indicating higher osteogenic potential on the NF scaffolds. ALP activity in TCPS+OS samples was significantly less than on NF samples at 14 d (Figure 5A). This result is not surprising as ALP expression is an early marker of osteogenic differentiation and is known to decrease as mineralization progresses [42]. MOD NF scaffolds did not have significantly higher ALP expression than SC or MOD SC films at 14 d (Figure 5A). These trends were further supported by 50 d alizarin red staining for calcified mineral.

After 50 d of culture, NF scaffolds showed strong alizarin red staining even without osteogenic supplement, demonstrating the ability of these scaffolds to support osteogenic differentiation (Figure 5B). MOD NF scaffolds however, did not show appreciable alizarin red staining, in accordance with their lower ALP expression at 14 d (Figure 5). In a complimentary study (Supplementary Figure S2) we found that MOD NF scaffolds could support hBMSC mineralization in the presence of osteogenic supplement. Both SC films and MOD SC films showed little to no signs of calcified mineral after 50 d of culture, similar to previously reported studies [14]. Positive TCPS+OS controls demonstrated a strong presence of calcified mineral, while negative TCPS controls did not have observable mineral deposition (Figure 5B).

Confocal fluorescence imaging of hBMSCs

Cell shape was investigated after 24 h of culture for cells on NF, MOD NF, SC and MOD SC scaffolds (Figure 6). 10 shape metrics were determined from snake outlines of the maximum projections of 63x/0.9 NA confocal z-stack images (n >35 cells per scaffold type). Significant differences between all possible pair wise comparisons were determined using a 1-Way ANOVA with Tukey's post-test (Table 1 and Supplementary Figure S3)for cell shape metric values. All cell shape metrics for NF vs SC scaffolds were significantly different ($p < 0.05$) except for aspect ratio ($p > 0.05$), which was significantly different between NF and MOD SC ($p < 0.05$). For NF vs. MOD NF, fewer significantly different metrics were identified, including regions of negative curvature ($p < 0.001$), tortuosity ($p < 0.01$), solidity ($p<0.01$) and aspect ratio ($p < 0.05$). The effect of scaffold chemistry on cell shape was more pronounced in the NF system compared to the SC system. For SC vs. MOD SC, there were no significant differences in cell shape metrics ($p > 0.05$) (Table 1). These results indicate a stronger dependence of cell shape on scaffold structure than on scaffold chemistry.

Human genome microarray

Microarray analysis of mRNA expression after 14 d of culture found a subset of 199 genes to be significantlyexpressed (passing a 1.5 fold, 10% filter) across all samples, relative to an average TCPS reference array (Figure 7A). Hierarchical clustering occurred within replicates with limited correlations across sample type. Through DAVID annotation cluster analysis, Biological process GO Terms relating to osteogenic phenotype were identified with a significant enrichment score of 2. 6 (Figure 7B). Further, the gene for alkaline phosphatase (ALPL) was present in this annotation cluster. *ALPL* $\log_2$fold change from TCPS (Figure 7C) was found to follow a similar trend to that seen in biochemical analysis of alkaline phosphatase activity at 14 d (Figure 5A). ALPL gene fold change was significantly higher on NF than that of MOD NF, MOD SC, and TCPS+OS. TCPS+OS ALPL fold change was negative indicating a decrease in *ALPL* expression at 14 d with osteogenic supplement. This result is in agreement with a decreased ALP activity for TCPS+OS seen with biochemical analysis at 14 d (Figure 5A).

Scaffolds were grouped into classes of ALL NF (NF and MOD NF), ALL SC (SC and MOD SC), ALL MOD (MOD NF and MOD SC), and ALL UN-MOD (NF and SC) for investigation of the effects of structure and chemistry on gene expression. SAM class comparisons were conducted on the 199 significantly expressed genes comparing ALL NF vs ALL SC and ALL MOD vs ALL UN-MOD. SAM analysis resulted in 16 differentially expressed genes between ALL NF and ALL SC, and 74 differentially expressed genes between ALL MOD vs ALL UN-MOD.

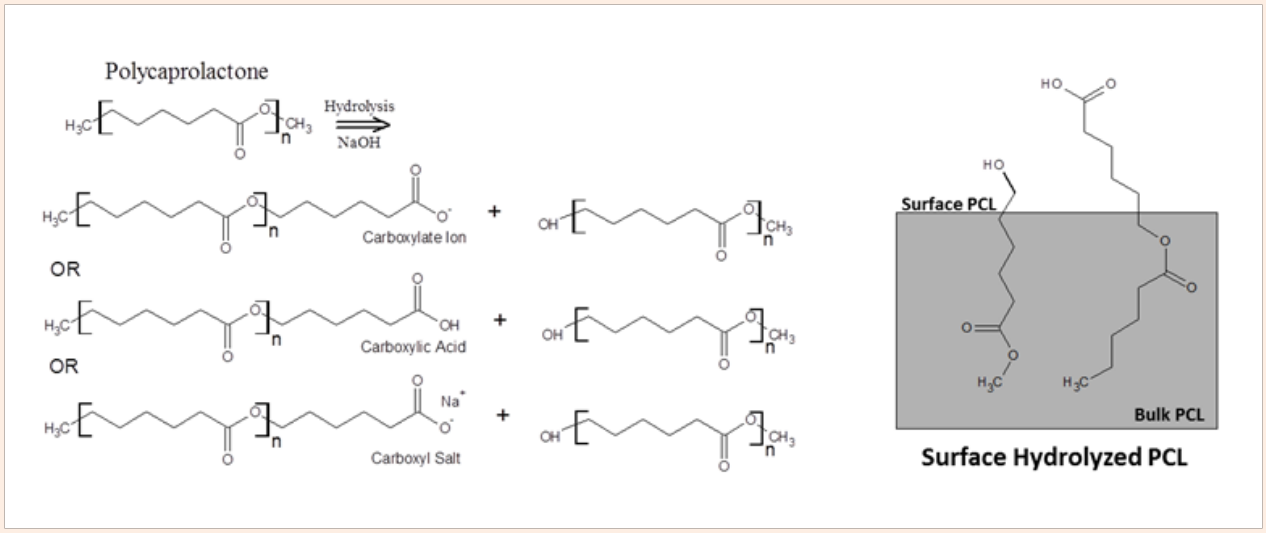

Figure 1: Schematic representation of PCL scaffold hydrolysis. PCL scaffolds are chemically modified by mild base hydrolysis in sodium hydroxide solution. Mild hydrolysis results in slight degradation of the polymer surface, opening surface carboxyl and hydroxyl groups. Carboxyl may be present in several forms including the carboxylate ion, carboxylic acid, and carboxyl salt.

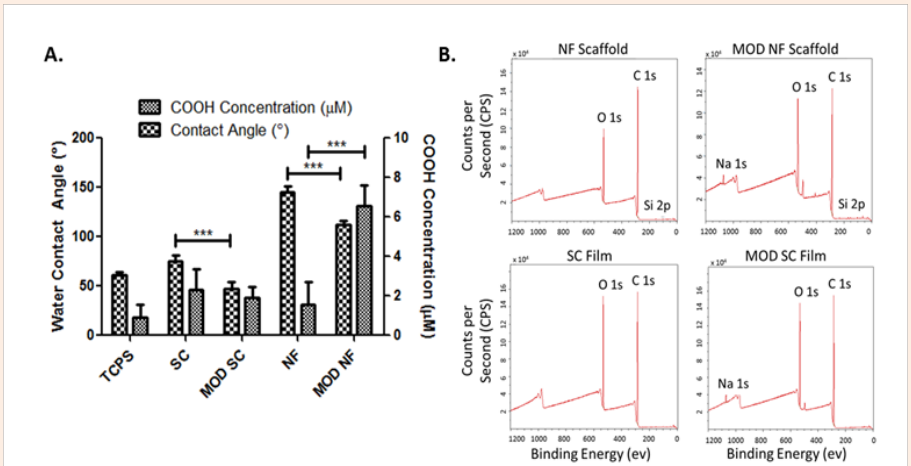

C.

	O 1S		C 1s		Na 1s		O 1s / C 1s	
	Ave At %	STDEV	Ave At %	STDEV	Ave At %	STDEV	Ave At % Ratio	STDEV
PCL Theoretical [CH2CH2CH2CH2CH2COO]	25		75		0		0.3	
NF Scaffold	17.5	0.4	82.1	0.3	0.0	0.0	0.214 *	0.005
MOD NF Scaffold	19.4	1.5	78.9	2.0	1.3	0.5	0.246 *	0.025
SC Film	21.8	0.1	78.3	0.1	0.0	0.0	0.278	0.001
MOD SC Film	21.7	0.1	77.0	0.2	0.4	0.3	0.282	0.001

Figure 2: (A) Contact angle and Carboxyl concentration. Water contact angle (left axis), and carboxyl concentration (right axis) measurements for TCPS controls, NF, MOD NF, SC, and MOD SC scaffolds. Error bars are standard deviation (S. D.) and statistically significant differences are represented by *** indicating $p < 0.001$ (1-way ANOVA with Tukey's Post Test, n = 4 samples per scaffold type). (B) XPS analysis of scaffold surface chemistry. Representative elemental survey scans of NF, MOD NF, SC, and MOD SC scaffolds. Detected elements are identified and listed with their corresponding position (binding energy, ev) and atomic percent (At %) concentration on the samples surface. (C) XPS elemental analysis of survey scans. Average and standard deviation calculated for each element detected (n = 9 (3 samples with 3 locations analyzed per sample)). Si was also detected from some samples but omitted from the table.

A.

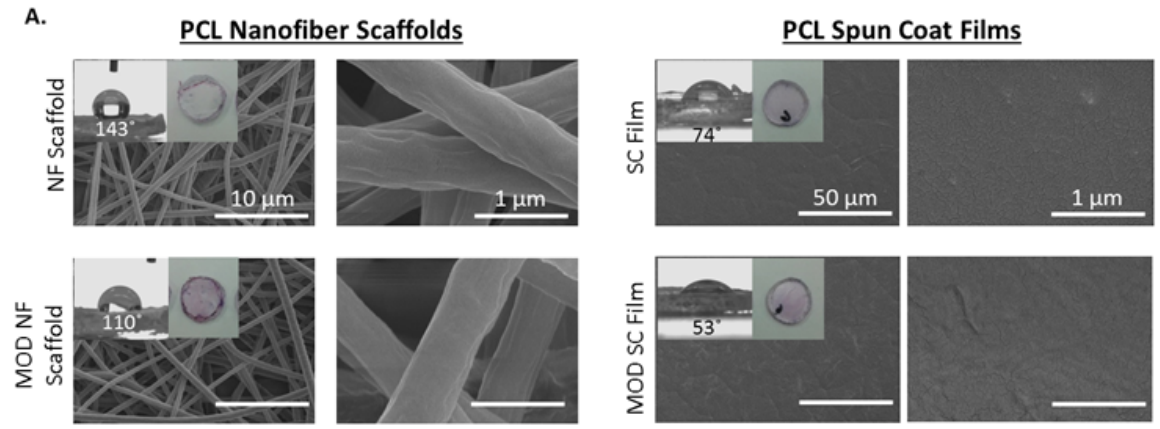

B.

Fiber Diameter (n > 70 Fibers)	NF Scaffolds	MOD NF Scaffolds
Mean (µm)	0.611	0.600
Std. Deviation (µm)	0.087	0.102
Minimum (µm)	0.302	0.344
Maximum (µm)	0.821	0.852
Coefficient of Variation (C_v)	0.142	0.169
Unpaired t-test to Compare Means	p = 0.46	
F-test to Compare Variances	p = 0.13	

Figure 3: (A) SEM of NF scaffold and SC film structural integrity with mild hydrolysis. SEM images were acquired at magnification 1,000, 5,000 and 50,000. Inlayed images are representative of contact angle measurements and staining of scaffold surface carboxyls with TBO reagent. (B) PCL nanofiber fiber diameter analysis. NF and MOD NF images taken at magnification 5,000 were used for analysis.

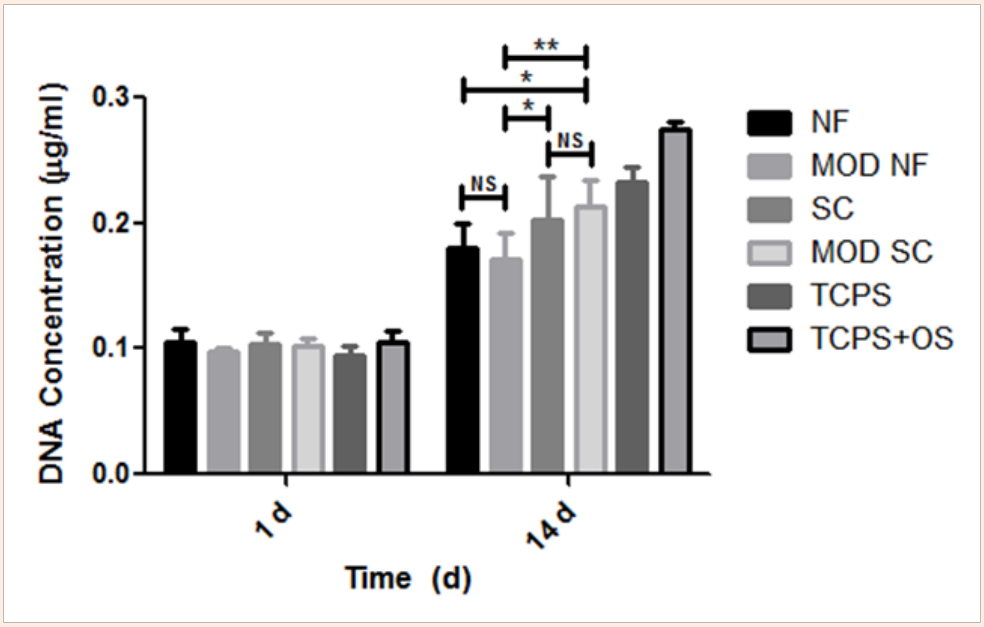

Figure 4: hBMSC DNA concentration after 1 d and 14 d of culture on NF, MOD NF, SC, and MOD SC scaffolds, and TCPS and TCPS+OS controls with cell seeding density of 10,000 cells/cm^2. Error bars are S. D. Statistical analysis with 2-way ANOVA with Bonferroni post test (* p<0. 05, ** p < 0. 01, NS p > 0. 05), (n = 4).

Citation: Sarkar S, Baker BA, ChenD, Pine PS, McDaniel JH, et al. (2016) Roles of Nanofiber Scaffold Structure and Chemistry in Directing Human Bone Marrow Stromal Cell Response. Adv Tissue EngRegen Med Open Access 1(1): 00003. DOI: 10.15406/atroa.2016.01.00003

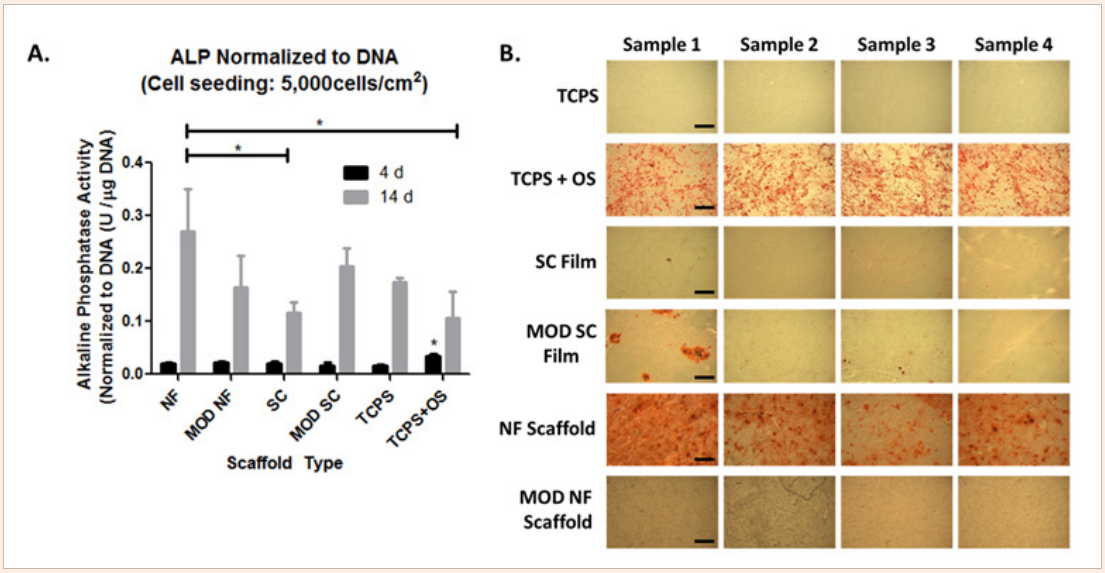

Figure 5: (A) Alkaline phosphatase activity (ALP). ALP activity is normalized to DNA concentration. Cells were seeded at a concentration of 5,000 cells/cm^2 and ALP measurements were taken at 4 d and 14 d. Error bars are S. D. and statistical analysis was conducted with a 1-way ANOVA with Tukey's Post-Test. (* $p < 0.05$, $n = 3$). (B) Alizarin Red Mineralization assay. Cells were seeded at a concentration of 10,000 cells/cm^2 and stained for mineralization at 50 d (mineral deposits stained red). Scale bar represents 500 µm.

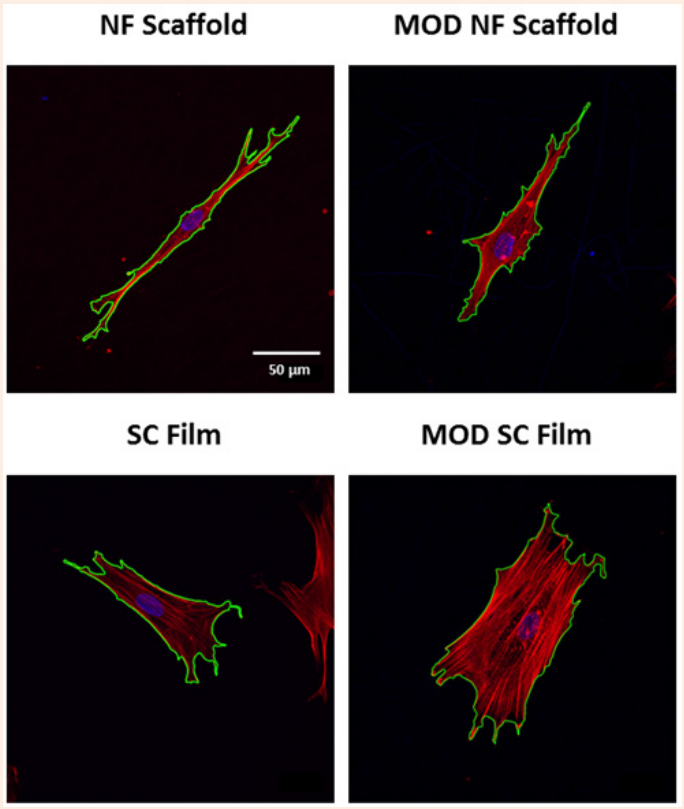

Figure 6: Maximum projection of confocal z-stacks of hBMSCs cultured for 24 h on NF, MOD NF, SC and MOD SC scaffolds. Images were taken using a magnification 63 water immersion lens. Maximum z-projections are shown with snake outlines (green), actin cytoskeleton (red) and nuclei (blue).

Citation: Sarkar S, Baker BA, ChenD, Pine PS, McDaniel JH, et al. (2016) Roles of Nanofiber Scaffold Structure and Chemistry in Directing Human Bone Marrow Stromal Cell Response. Adv Tissue EngRegen Med Open Access 1(1): 00003. DOI: 10.15406/atroa.2016.01.00003

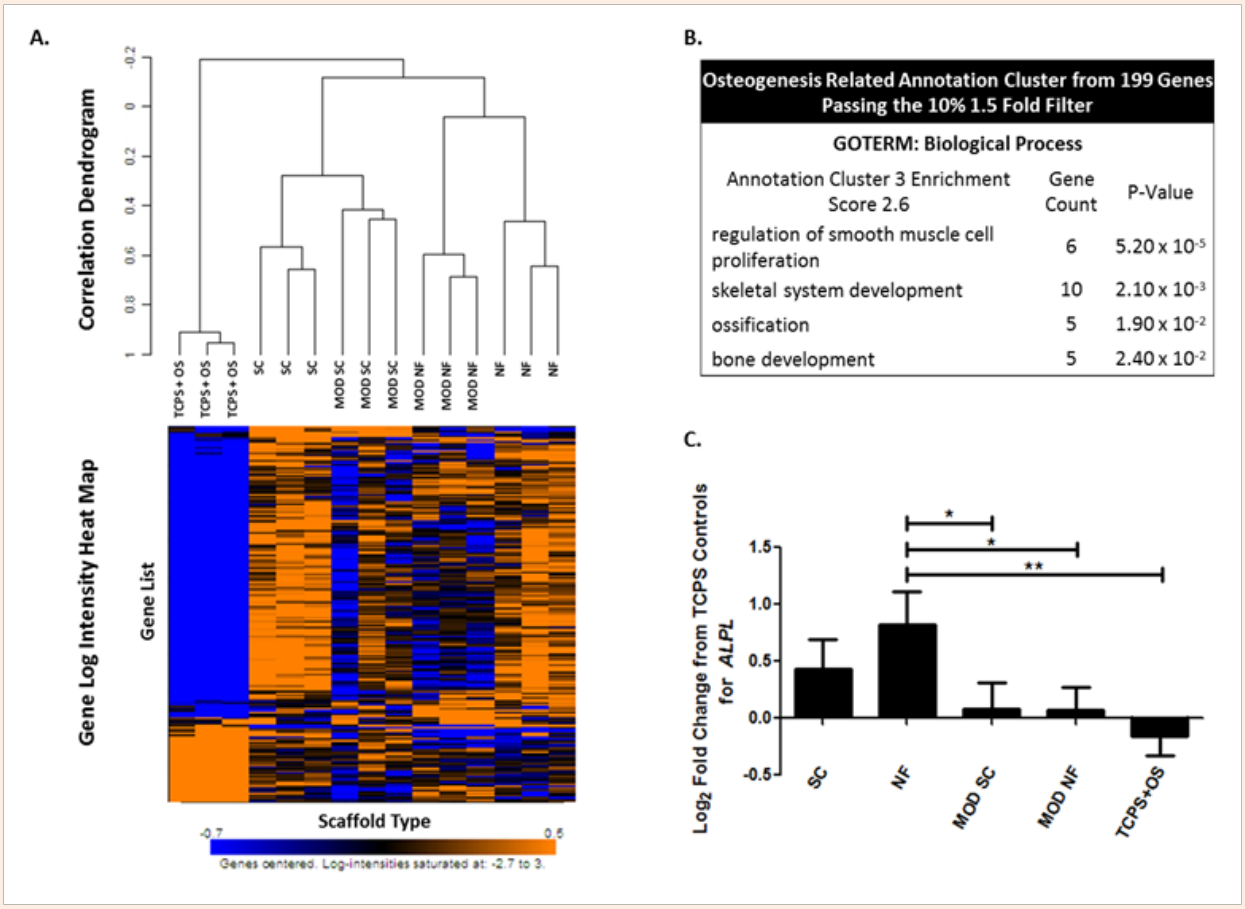

Figure 7: (A) Dendrogram and heat map of significantly expressed genes. Genes were normalized to an average TCPS reference array. From 47,231 genes, a subset of 199 genes was found to exhibit at least a 1. 5-fold change from the genes median value. Hierarchical clustering analysis (HCA), with centered correlation and average linkage, was performed using all arrays (except the TCPS control arrays) and the 199 1. 5-fold significant genes. Correlation dendrogram was generated from hierarchical clustering of samples with gene centered analysis. (B) Annotation cluster 3 related to osteogenic response, from DAVID annotation clustering of the 199 significant genes. (C) Log_2 fold change from TCPS for alkaline phosphatase (bone/liver/kidney) *(ALPL)* gene, enriched in the annotation cluster presented in (B). Statistical differences were analyzed using one-way ANOVA with Tukey's multiple comparisons post-test (* p<0. 05, ** p < 0. 01, n = 3).

Annotation cluster analysis of GO term enriched from ALL NF vs ALL SC genes resulted in one significant annotation cluster(enrichment score of 2.0). The annotation cluster contained GO terms related to extracellular regions, parts, and matrix as well as proteinaceous extracellular matrix (Table 2). Genes found in this annotation cluster are presented in Figure 8A as log_2 fold change from TCPS. ECM related genes, *COL8A2*,*FNDC1*, *FBLN5*, and *GPC4*, were all found to be down regulated on SC films, regardless of chemical modification, while these genes were up regulated on NF scaffolds regardless of chemical modification (Figure 8A). *IGFBP1*which promotes cell migration and alters the interaction of IGFs with cell surface receptors [43]was up regulated in SC and MOD SC films while it was minimally regulated in NF and MOD NF scaffolds. IL 8, generally released in response to inflammatory stimulus [44], was largely up regulated in SC, MOD SC, and NF scaffolds while it was not regulated in MOD NF scaffolds (Figure 8A).

Annotation cluster analysis of KEGG pathways enriched from ALL MOD vs ALL UN-MOD genes resulted in pathways primarily related to glycolysis/gluconeogenesis and sugar metabolism (Table 2). Also enriched was a KEGG pathway related to pathogenic *Escherichia coli (E.coli)* infection, however, the specific genes enriched from SAM analysis are also related to actin cytoskeletal reorganization. Biological process GO term cluster analysis also similarly resulted in significantly enriched clusters related to glycolysis, sugar processing and cell migration/locomotion (Table 2). The specific genes found in the enriched KEGG pathways are presented in Figures 8B and 8C. KEGG pathway genes related to glycolysis and sugar processing were found to be generally up-regulated or minimally-regulated in NF and SC scaffolds, however they are largely down-regulated in MOD NF and MOD SC scaffolds (Figure 8B).

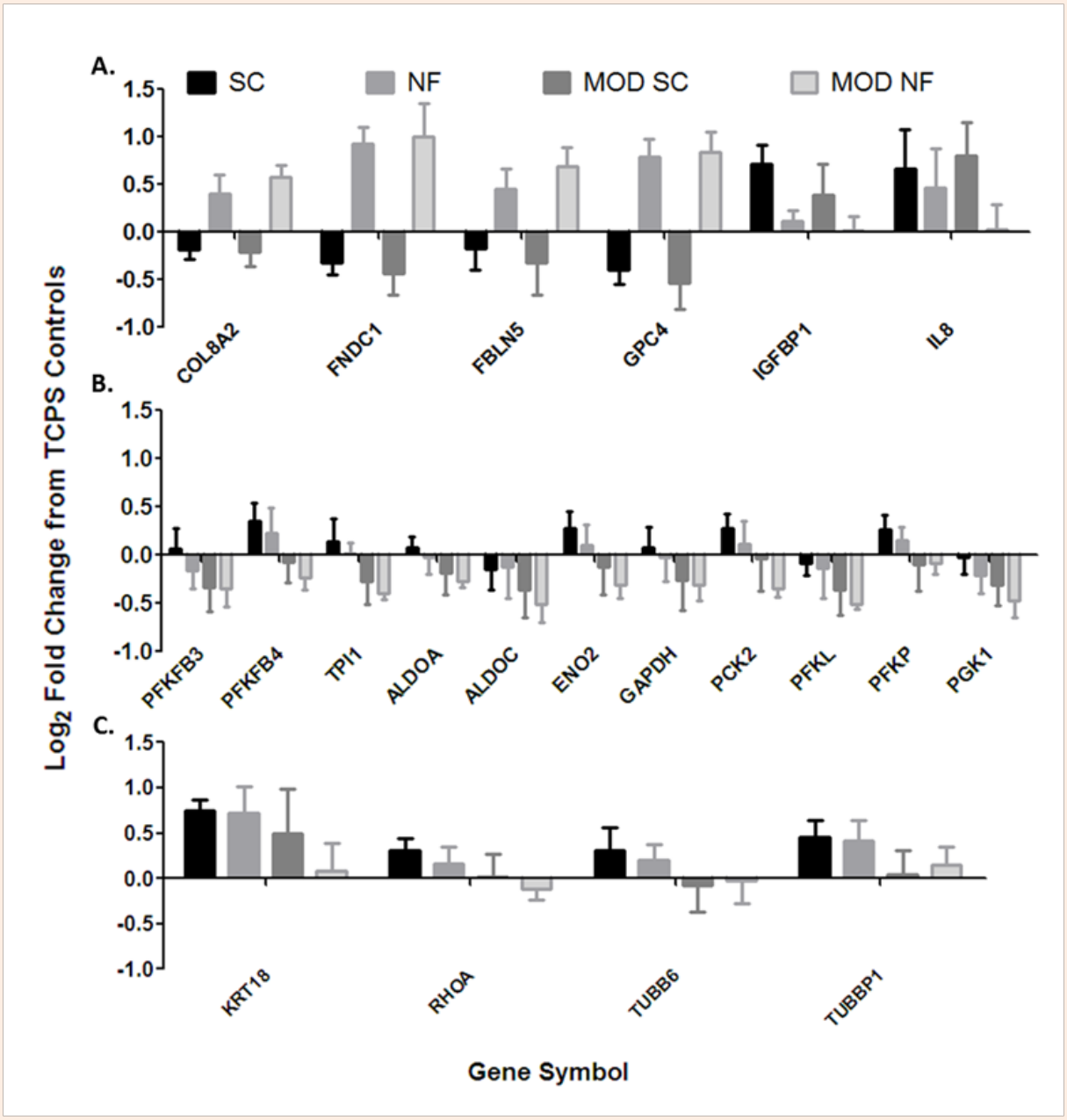

Figure 8: $\log_2$ fold change from TCPS for (A) genes enriched in annotation cluster 1 in DAVID analysis of differentially expressed genes in the ALL NF vs ALL SC SAMs class comparison (ALL NF combines NF and MOD NF scaffolds while ALL SC combines SC and MOD SC scaffolds). (B) Genes enriched in metabolic KEGG pathways for the ALL MOD vs ALL Un-MOD Comparison. (C) Genes related to cytoskeleton enriched in the KEGG pathway for the ALL MOD vs ALL Un-MOD Comparison.

Several genes related to cytoskeletal organization were also significantly enriched into KEGG pathways: *KRT18* (keratin 18), *RHOA* (ras homolog gene family, member A), *TUBB6* (tubulin, beta 6), and *TUBBP1* (similar to tubulin, beta 5). These genes were identified as a part of the pathogenic *Escherichia coli* infection KEGG pathway, however, these genes also strongly associate with the cytoskeleton gene ontology for cellular components (Gene count 4, p-value of 0.0013). There were no infection related genes identified as a part of the *E.coli* pathway, suggesting that the regulation of these cytoskeletal genes was not a result of infection. Cytoskeleton related genes were consistently up-regulated in un-modified scaffolds while they were minimally-regulated or down-regulated in modified scaffolds (Figure 8C).

Table 1: Summary of significant difference in cell shape metrics. Shape metrics were determined from snake outlines of hBMSCs cultured on scaffolds of varying chemistry and structure. Statistical differences across four scaffold groups were analyzed using 1-way ANOVA with Tukey's multiple comparisons post-test (ns $p > 0.05$, * $p < 0.05$, ** $p < 0.01$, *** $p < 0.001$, $n > 35$)*

	Area (μm^2)	Perimeter (μm)	Mean Boundary Distance(μm)	Mean Negative Curvature (μm^{-1})	Regions of Negative Curvature	Tortuosity	Circularity	Solidity	Aspect Ratio	Minor Axis Length (μm)
NF vs. MOD NF	ns	ns	ns	ns	***	**	ns	**	*	ns
NF vs. SC	***	**	***	**	*	**	***	***	ns	***
NF vs. MOD SC	***	ns	**	***	ns	***	***	***	*	***
MOD NF vs. SC	***	**	*	**	ns	**	**	ns	***	***
MOD NF vs. MOD SC	***	ns	ns	***	ns	**	***	**	***	***
SC vs. MOD SC	ns	ns	ns	ns	ns	ns	ns	ns	ns	ns

NF: PCL Non-Woven Nanofibers; SC films: PCL Spin-Coated TCPS Discs; MOD NF: NF Scaffolds Modified by Mild Hydrolysis; MOD SC: SC Films Modified by Mild Hydrolysis.

Table 2: Functional Annotation Clustering using DAVID analysis of genes differentially expressed between ALL NF vs ALL SC (16 genes found) and between ALL MOD vs ALL UN-MOD (79 genes found). "ALL NF" combines gene expression data from NF and MOD NF, "ALL SC" combines SC and MOD SC, "All MOD" combines MOD NF and MOD SC, and "ALL UN-MOD" combines NF and SC*.

Effect of Structure: All NF vs. All SC (Regardless of Chemistry)		
GOTERM: Cellular Components		
Annotations cluster 1 Enrichment Score 2. 0	**Gene Count**	**P-Value**
Extracellular region part	5	0. 0017
Extracellular region	6	0. 0035
Proteinaceous extracellular matrix	3	0. 016
Extracellular matrix	3	0. 018
Effect of Chemistry: ALL MOD vs. ALL UN-MOD(Regardless of structure)		
KEGG Pathway	**Gene Count**	**P-Value**
Glycolysis/ Gluconeogensis	9	1.5×10^{-9}
Fructose and mannose metabolism	7	3.7×10^{-8}
Pentose phosphate pathway	4	4.3×10^{-4}
GOTERM: Biological process		
Annotation Cluster 1 Enrishment Score: 7. 6	**Gene Count**	**P-Value**

Glycolysis	8	2.9×10^{-10}
Monosaccharide metabolic process	12	3.1×10^{-10}
Hexose metabolic process	11	1.3×10^{-9}
Annotation Cluster 2 Enrishment score: 2. 8	**Gene Count**	**P-Value**
Monosaccharide biosynthesis process	4	3.2×10^{-4}
Pyruvate metabolic process	4	4.6×10^{-4}
Alcohol biosynthesis process	4	5.3×10^{-4}
Annotation Cluster 3 Enrishment score: 2. 1	**Gene Count**	**P-Value**
Carboxylic acid biosynthesis process	5	0. 0024
Organic acid biosynthesis process	5	0. 0024
Amine biosynthesis process	4	0. 0031
Annotation Cluster 4 Enrishment score: 1. 3	**Gene Count**	**P-Value**
Protein oligomerization	4	0. 0025
Protein complex biogenesis	6	0. 0035
Protein complex assembly	6	0. 0035
Annotation Cluster 5 Enrishment score: 1. 3	**Gene Count**	**P-Value**
Negative regulation of cell migration	3	0. 018
Negative regulation of locomotion	3	0. 021
Negative regulation of cell motion	3	0. 022

NF: PCL Non-Woven Nanofibers, SC films: PCL Spin-Coated TCPS Discs; MOD NF: NF Scaffolds Modified by Mild Hydrolysis; MOD SC: SC Films Modified by Mild Hydrolysis; MOD SC: SC Films Modified by Mild Hydrolysis; ALL NF: NF and MOD NF; ALL SC: SC and MOD SC; ALL MOD: MOD NF and MOD SC; ALL UN-MOD: NF and SC; KEGG: Kyoto Encyclopedia of Genes and Genomes; GOTERM: Gene Ontology Term.

Discussion

Nanofiber scaffolds have shown particular promise in bone tissue engineering and regenerative medicine strategies. Enhanced differentiation of stem cells in nanofiber scaffolds has been previously demonstrated, however the material properties and cellular mechanisms driving this process are largely unknown [7,9-13]. In this study, we have comprehensively investigated hBMSC response to nanofiber scaffolds of different chemistry to examine the contributions of scaffold structure and chemistry on stem cell response.

To minimize differences in nanofiber scaffold structure while varying nanofiber chemistry, we employed a wet chemical method to modify the nanofiber mat surface after the formation of fibers. After mild hydrolysis with NaOH treatment, nanofiber scaffolds demonstrated decreased water contact angle with concurrent increase in –COOH functional groups on the scaffold surface while

SEM images indicated there were no significant changes to fiber diameter or overall nanofiber scaffold structure. PCL spun coat films were also investigated to serve as 2-D substrate analogs of the nanofiber scaffolds. Overall, a water contact angle decrease of approximately 33°C was seen on MOD NF scaffolds while a decrease of approximately 27°C was detected on MOD SC films. It has been previously reported that changes in water contact angle of this magnitude on 2-D surfaces can produce relevant changes in cell behaviors such as cell shape, attachment, proliferation and differentiation [45,46].

Modification of the nanofiber scaffold surface chemistry resulted in significant changes to hBMSC osteogenic differentiation. hBMSCs on MOD NF scaffolds did not show the characteristic osteogenic response (elevated alkaline phosphatase activity and mineralization) generally observed on NF scaffolds (Figure 5) [14]. A decrease in osteogenic response with the introduction of surface -COOH/-OH functional groups on the nanofiber scaffolds is consistent with reports for 2-D -COOH functionalized materials. In a study by Keselowsky et al. [39], self-assembled monolayers of varying functionality were coated with fibronectin then investigated for their effect on the expression of osteoblast specific genes by MC3T3-E1 cells. They found that gene markers for ALP, bone sialoprotein and osteocalcin were all down regulated on -COOH surfaces [39]. Similarly, Curran et al. [44] found that 2-D –OH and -COOH surfaces did not support osteogenesis of bone-marrow-derived mesenchymal stem cell while they did promote chondrogenesis[44]. These results suggest that the nanofiber scaffold structural cues cannot overcome surface chemistry cues for cell response.

The current material system provides a unique opportunity to investigate the mechanisms behind osteogenic differentiation in nanofiber scaffolds. One possible mechanism is the influence of scaffold architecture on cell shape [14,46]. Several studies have demonstrated a possible correlation between cell shape and stem cell differentiation [47-50]. In nanofiber scaffolds particularly, Kumar et al. [14] noted that 1 day hBMSC shape was similar to that on flat substrates treated with osteogenic supplements and suggested that the osteoinductive effects of nanofibers come from their ability to elicit an osteogenic morphology [14]. In our system, we were able to investigate cell shapes in nanofiber scaffolds that are associated with both osteogenic, and non-osteogenic outcomes. In the NF scaffold, we observe positive expression of markers associated with osteogenic differentiation, while in the MOD NF scaffold markers of osteogenic differentiation are reduced or show limited expression. Interestingly, in investigating 1 d cell shape between the two materials, we find that only a few metrics are significantly different, while the majority of metrics are unaltered by the chemical modification and subsequent state of hBMSC differentiation.

Metrics found to be significantly different between NF and MOD NF includes regions of negative curvature, tortuosity, solidity, and to a lesser extent aspect ratio (Table 1). These metrics which are significantly different between cells in an osteogenic nanofiber environment and a non-osteogenic nanofiber environment may be possible targets for the use of cell shape metrics in the prediction of osteogenic differentiation in nanofiber scaffolds. On the other hand, metrics such as cell projected area, perimeter and circularity have been demonstrated here to not be strongly correlated with osteogenic differentiation in the nanofiber system. These results differ from that seen in flat 2-D culture environments, where the analogous metrics of cell spread area and roundness were found to be strongly correlated to stem cell lineage commitment [48]. Therefore, specific cell metrics relevant to differentiation in 2-D may not directly translate to a more 3-D topographical system where the scaffold architecture is dominant in determining cell shape.

In our material system we can also investigate the relative contributions of structure and chemistry in directing stem cell response. Through microarray gene expression analysis, we find that ECM related pathways are more affected by scaffold structure while metabolic and cytoskeletal related pathways are more affected by scaffold surface chemistry. Although gene expression values from microarray data are only semi-quantitative, genes identified in these pathways provide candidates for future investigation (through PCR and immune staining) of specific cellular mechanisms that may be associated with hBMSC response to nanofiber scaffold properties.

ECM related genes (*COL8A2, FNDC1, FBLN5*and *GPC4*) were generally up-regulated on all NF scaffolds (NF and MOD NF) regardless of scaffold surface chemistry (Figure 8A). In contrast, the same genes are consistently down-regulated on spun coat films (SC and MOD SC). Interestingly, the up-regulation of ECM related genes has been demonstrated to be correlated with *in vivo* bone forming phenotype of hBMSCs[51]. Lui et al. [52] also investigated microarray gene expression analysis of hBMSCs in nanofiber scaffolds and found ECM GO Terms to be significantly enriched on nanofiber mats [52]. Surprisingly, in our study, the regulation of ECM related genes was independent of the osteogenic outcome (Figure 5B). These results suggest that scaffold structure (NF versus SC Film) is a dominant scaffold feature in ECM related gene regulation, but not necessarily *in vitro*osteogenic response.

Scaffold surface chemistry was found to influence gene expression in pathways related to glycolysis/gluconeogenesis and other metabolic pathways (Table 2). Scaffold chemical modification (mild hydrolysis inducing –COOH/-OH groups) resulted in down-regulation of genes associated with glycolysis/gluconeogenesis and metabolism regardless of scaffold structure (Figure 8B)whereas, only un-modified scaffolds showed up-regulation of several of these genes (*PFKFB4, TPI1, ENO2, PCK2*, and *PFKP*). It should be noted that the glycolysis/gluconeogenesis pathway shares many overlapping genes with other pathways, making interpretation of the functional outcome of these results difficult. For example, the adolase family of genes is also associated with gene ontologies related to actin cytoskeleton and cytoskeletal binding and have been implicated in the regulation of cell contraction [53]. Scaffold chemistry resulted in regulation of these related genes independent of both scaffold structure and osteogenic response (Figure 8B).

Surface chemistry and hydrophilicity affect both the amount of adsorbed serum proteins as well as the conformation of proteins at the cell-biomaterial interface [54-57]. The increase of surface carboxyl groups in particular has been associated with increased

protein adsorption from serum containing culture media as well as conformational changes in the adsorption of specific proteins such as fibronectin [54-57]. It is possible that the presence of carboxyl and hydroxyl groups on the modified nanofiber and spun coat film surfaces may have altered protein adsorption to the scaffold, thereby altering the presentation of key proteins, cytokines and growth factors related to signaling in the metabolic pathways.

In addition to the enrichment of metabolic pathways, expression of genes related to the cytoskeleton was also influenced by surface chemistry. *KRT18*, *RHOA*, *TUBB6*, and *TUBBP1* were generally found to be up regulated in NF and SC scaffolds while these genes had relatively low expression in the MOD NF and MOD SC scaffolds (Figure 8C) indicating an influence on cytoskeletal organization by –COOH/-OH chemical modification. Cytoskeletal regulation is consistent with our finding that cell shape is moderately affected by nanofiber chemical modification. Although cell shape was more strongly affected by scaffold structure (NF vs SC) (Table 1), genomic regulation of the cytoskeleton in UN-MOD vs MOD scaffolds indicates changes in the cytoskeleton as a possible mechanism through which scaffold chemistry may alter stem cell function. In particular, cell shape was demonstrated by McBeath et al. [48] to play an integral role in stem cell linage commitment through the modulation of RhoA activity as well as the generation of cytoskeletal tension [48]. In our study, we find that *RHOA* is up-regulated in the un-modified scaffolds (NF and SC) while it is minimally expressed or even down- regulated (MOD SC and MOD NF) in the modified scaffolds relative to TCPS controls (Figure 8C). The RhoA pathway as well as the generation or disruption of cytoskeletal tension should be further investigated as a possible mechanism underlying scaffold chemistry-related modulation of stem cell lineage commitment.

Conclusion

We have developed a material system that allows investigation of the effects of both scaffold structure and chemistry in regulating stem cell response in the nanofiber scaffold environment. The nanofiber environment can promote osteogenic differentiation; however, alterations in scaffold chemistry can modulate this response. Nanofiber surface chemical modification with COOH/OH via mild hydrolysis results in reduced osteogenic response from hBSMCs. These studies suggest that both nanofiber scaffold structure and chemistry should be carefully engineered in order to achieve a desired biological response. Cell response to modified nanofiber scaffolds are reflected in changes to cell shape, cytoskeletal rearrangement and metabolic changes. Nanofiber scaffold structure was found to influence cell shape and ECM gene expression; however, these cellular responses may not be directly correlated to osteogenic response. The MOD NF scaffolds provide a negative control for osteogenic differentiation in the NF scaffold system, thereby allowing for further investigation into the mechanisms behind nanofiber scaffold mediated osteogenic differentiation.

Acknowledgement

S.Sarkar was supported by the National Research Council-NIST postdoctoral fellowship. B. A.Baker was supported by the National Research Council-ARRA-NIST postdoctoral fellowship. Thank you to Christopher M. Stafford, NIST, for assistance with XPS.

Copyright Disclaimer

References

1. Dvir T, Timko BP, Kohane DS, Langer R (2011) Nanotechnological strategies for engineering complex tissues. Nat Nano 6(1): 13-22.
2. Bhardwaj N, Kundu SC (2010) Electrospinning: A fascinating fiber fabrication technique. Biotechnol Adv 28(3): 325-347.
3. Beachley V, Wen X (2010) Polymer nanofibrous structures: Fabrication, biofunctionalization, and cell interactions. Prog Polym Sci 35(7): 868-892.
4. Mao HQ, Lim SH, Zhang S, Christopherson G, Kam K, et al. (2010) Biomaterials as Stem Cell Niche: The nanofiber matrix as an artificial stem cell niche. In: Krishnendu Roy (Ed.), Studies in Mechanobiology, Tissue Engineering and Biomaterials. Springer Berlin Heidelberg, USA, pp. 89-118.
5. Rieger KA, Birch NP, Schiffman JD (2013) Designing electrospun nanofiber mats to promote wound healing a review. J Mater Chem B 1: 4531-1441.
6. Smith Callahan LA, Xie S, Barker IA, Zheng J, Reneker DH, et al. (2013) Directed differentiation and neurite extension of mouse embryonic stem cell on aligned poly (lactide) nanofibers functionalized with yigsr peptide. Biomaterials 34(36): 9089-9095.
7. Chua KN, Chai C, Lee PC, Tang YN, Ramakrishna S, et al. (2006) Surface aminated electrospun nanofibers enhance adhesion and expansion of human umbilical cord blood hematopoietic stem/progenitor cells. Biomaterials 27(36): 6043-6051.
8. Yoo HS, Kim TG, Park TG (2009) Surface functionalized electrospun nanofibers for tissue engineering and drug delivery. Adv Drug Deliv Rev 61(12): 1033-1042.
9. Ruckh TT, Kumar K, Kipper MJ, Popat KC (2010) Osteogenic differentiation of bone marrow stromal cells on poly(ε-caprolactone) nanofiber scaffolds. Acta Biomater 6(8): 2949-2959.
10. Gandhimathi C, Venugopal J, Ravichandran R, Sundarrajan S, Suganya S, et al. (2013) Mimicking nanofibrous hybrid bone substitute for mesenchymal stem cells differentiation into osteogenesis. Macromol Biosci 13(6): 696-706.
11. Yu HS, Jang JH, Kim TI, Lee HH, Kim HW (2009) Apatite mineralized polycaprolactone nanofibrous web as a bone tissue regeneration substrate. J Biomed Mater Res A 88(3): 747-754.
12. Yoshimoto H, Shin Y, Terai H, Vacanti J (2003) A biodegradable nanofiber scaffold by electrospinning and its potential for bone tissue engineering. Biomaterials 24(12): 2077-2082.
13. Shin SH, Purevdorj O, Castano O, Planell JA, Kim HW (2012) A short review: Recent advances in electrospinning for bone tissue regeneration. J Tissue Eng 3(1): 2041731412443530.
14. Kumar G, Tison CK, Chatterjee K, Pine PS, McDaniel JH, et al. (2011) The determination of stem cell fate by 3d scaffold structures through the control of cell shape. Biomaterials 32(35): 9188-9196.
15. Araujo J, Martins A, Leonor I, Pinho E, Reis R, et al. (2008) Surface controlled biomimetic coating of polycaprolactone nanofiber meshes

to be used as bone extracellular matrix analogues. J Biomater Sci Polym Ed 19(10): 1261-1278.

16. Martins A, Pinho ED, Faria S, Pashkuleva I, Marques AP, et al. (2009) Surface modification of electrospun polycaprolactone nanofiber meshes by plasma treatment to enhance biological performance. Small 5(10): 1195-1206.
17. Park K, Ju YM, Son JS, Ahn KD, Han DK (2007) Surface modification of biodegradable electrospun nanofiber scaffolds and their interaction with fibroblasts. J Biomater Sci Polym Ed 18(4): 369-382.
18. Liu W, Cai Q, Zhang F, Wei Y, Zhang X, et al. (2013) Dose dependent enhancement of bone marrow stromal cells adhesion, spreading and osteogenic differentiation on atmospheric plasma-treated poly(l-lactic acid) nanofibers. Journal of Bioactive and Compatible Polymers 28(5): 453-467.
19. Oyane A, Uchida M, Choong C, Triffitt J, Jones J, et al. (2005) Simple surface modification of poly(ε-caprolactone) for apatite deposition from simulated body fluid. Biomaterials 26(15): 2407-2413.
20. Lam CXF, Teoh SH, Hutmacher DW (2007) Comparison of the degradation of polycaprolactone and polycaprolactone (β-tricalcium phosphate) scaffolds in alkaline medium. Polymer International 56(6): 718-728.
21. Lam CXF, Savalani MM, Teoh SH, Hutmacher DW (2008) Dynamics of in vitro polymer degradation of polycaprolactone based scaffolds: Accelerated versus simulated physiological conditions. Biomed Mater 3(3): 034108.
22. Sano S, Kato K, Ikada Y (1993) Introduction of functional groups onto the surface of polyethylene for protein immobilization. Biomaterials 14(11): 817-822.
23. Ying L, Yin C, Zhuo R, Leong K, Mao H, et al. (2003) Immobilization of galactose ligands on acrylic acid graft-copolymerized poly (ethylene terephthalate) film and its application to hepatocyte culture. Biomacromolecules 4(1): 157-165.
24. Gupta B, Hilborn JG, Bisson I, Frey P (2001) Plasma induced graft polymerization of acrylic acid onto poly(ethylene terephthalate) films. Journal of Applied Polymer Science 81(12): 2993-3001.
25. Chong Seow KM (2010) Development of cell sheet constructs for layer by layer tissue engineering using the blood vessel as an experimental model. National University of Singapore, Singapore.
26. Ma Z, He W, Yong T, Ramakrishna S (2005) Grafting of gelatin on electrospun poly (caprolactone) nanofibers to improve endothelial cell spreading and proliferation and to control cell orientation. Tissue Eng 11(7-8): 1149-1158.
27. Xu C, Prince JL (1998) Snakes, shapes, and gradient vector flow. Image Processing, IEEE Transactions 7(3): 359-369.
28. Driscoll MK, Albanese JL, Xiong ZM, Mailman M, Losert W, et al. (2012) Automated image analysis of nuclear shape: What can we learn from a prematurely aged cell? Aging (Albany NY) 4(2): 119-132.
29. Driscoll MK, Fourkas JT, Losert W (2011) Local and global measures of shape dynamics. Phys Biol 8(5): 055001.
30. Tusher VG, Tibshirani R, Chu G (2001) Significance analysis of microarrays applied to the ionizing radiation response. Proc Natl Acad Sci 98(9): 5116-5121.
31. Huang DW, Sherman BT, Lempicki RA (2009) Bioinformatics enrichment tools: Paths toward the comprehensive functional analysis of large gene lists. Nucleic Acids Res 37(1): 1-13.
32. Huang da W, Sherman BT, Lempicki RA (2009) Systematic and integrative analysis of large gene lists using david bioinformatics resources. Nat Protoc 4(1): 44-57.
33. Ogata H, Goto S, Sato K, Fujibuchi W, Bono H, et al. (1999) Kegg: Kyoto encyclopedia of genes and genomes. Nucleic Acids Res 27(1): 29-34.
34. Quackenbush J (2002) Microarray data normalization and transformation. Nat Genet 32: 496-501.
35. Huang F, Wang Q, Wei Q, Gao W, Shou H, et al. (2010) Dynamic wettability and contact angles of poly (vinylidene fluoride) nanofiber membranes grafted with acrylic acid. Express Polym Lett 4(9): 551-558.
36. Wagner MS, McArthur SL, Shen M, Horbett TA, Castner DG (2002) Limits of detection for time of flight secondary ion mass spectrometry (tof-sims) and x-ray photoelectron spectroscopy (xps): Detection of low amounts of adsorbed protein. J Biomater Sci Polym Ed 13(4): 407-428.
37. Ratner BD, Castner DG (2009) Electron spectroscopy for chemical analysis. Surface Analysis-The Principal Techniques. (2nd edn), pp. 47-112.
38. Croll TI, O Connor AJ, Stevens GW, Cooper White JJ (2004) Controllable surface modification of poly(lactic-co-glycolic acid) (plga) by hydrolysis or aminolysis i: Physical, chemical, and theoretical aspects. Biomacromolecules 5(2): 463-473.
39. Keselowsky BG, Collard DM, García AJ (2005) Integrin binding specificity regulates biomaterial surface chemistry effects on cell differentiation. Proc Natl Acad Sci 102(17): 5953-5957.
40. Golub EE, Boesze Battaglia K (2007) The role of alkaline phosphatase in mineralization. Current Opinion in Orthopaedics, 18(5): 444-448.
41. Aubin JE (2001) Regulation of osteoblast formation and function. Rev Endocr Metab Disord 2(1): 81-94.
42. Jones JI, Gockerman A, Busby WH, Wright G, Clemmons DR (1993) Insulin like growth factor binding protein 1 stimulates cell migration and binds to the alpha 5 beta 1 integrin by means of its arg-gly-asp sequence. Proc Natl Acad Sci 90(22): 10553-10557.
43. Baggiolini M, Clark Lewis I (1992) Interleukin 8, a chemotactic and inflammatory cytokine. FEBS Letters 307(1): 97-101.
44. Curran JM, Chen R, Hunt JA (2006) The guidance of human mesenchymal stem cell differentiation in vitro by controlled modifications to the cell substrate. Biomaterials 27(27): 4783-4793.
45. Kennedy SB, Washburn NR, Simon Jr CG, Amis EJ (2006) Combinatorial screen of the effect of surface energy on fibronectin mediated osteoblast adhesion spreading and proliferation. Biomaterials 27(20): 3817-3824.
46. Kumar G, Waters MS, Farooque TM, Young MF, Simon Jr CG (2012) Freeform fabricated scaffolds with roughened struts that enhance both stem cell proliferation and differentiation by controlling cell shape. Biomaterials 33(16): 4022-4030.
47. Kolind K, Leong KW, Besenbacher F, Foss M (2012) Guidance of stem cell fate on 2d patterned surfaces. Biomaterials 33(28): 6626-6633.
48. McBeath R, Pirone DM, Nelson CM, Bhadriraju K, Chen CS (2004) Cell shape, cytoskeletal tension, and rhoa regulate stem cell lineage commitment. Dev Cell 6(4): 483-495.
49. Rodríguez JP, González M, Ríos S, Cambiazo V (2004) Cytoskeletal organization of human mesenchymal stem cells (msc) changes during

their osteogenic differentiation. J Cell Biochem 93(4): 721-731.

50. Treiser MD, Yang EH, Gordonov S, Cohen DM, Androulakis IP, et al. (2010) Cytoskeleton-based forecasting of stem cell lineage fates. Proc Natl Acad Sci 107(2): 610-615.

51. Larsen KH, Frederiksen CM, Burns JS, Abdallah BM, Kassem M (2010) Identifying a molecular phenotype for bone marrow stromal cells with in vivo bone-forming capacity. J Bone Miner Res 25(4): 796-808.

52. Liu W, Wei Y, Zhang X, Xu M, Yang X, Deng X (2013) Lower extent but similar rhythm of osteogenic behavior in hbmscs cultured on nanofibrous scaffolds versus induced with osteogenic supplement. ACS Nano 7(8): 6928-6938.

53. Kusakabe T, Motoki K, Hori K (1997) Mode of interactions of human aldolase isozymes with cytoskeletons. Arch Biochem Biophys 344(1): 184-193.

54. Keselowsky BG, Collard DM, García AJ (2005) Integrin binding specificity regulates biomaterial surface chemistry effects on cell differentiation. Proc Natl Acad Sci 102(17): 5953.

55. Keselowsky BG, Collard DM, García AJ (2003) Surface chemistry modulates fibronectin conformation and directs integrin binding and specificity to control cell adhesion. J Biomed Mater Res A 66(2): 247-259.

56. Arima Y, Iwata H (2007) Effect of wettability and surface functional groups on protein adsorption and cell adhesion using well-defined mixed self-assembled monolayers. Biomaterials 28(20): 3074-3082.

57. Arima Y, Iwata H (2007) Effects of surface functional groups on protein adsorption and subsequent cell adhesion using self-assembled monolayers. J Mater Chem 17(38): 4079-4087.

Citation: Sarkar S, Baker BA, ChenD, Pine PS, McDaniel JH, et al. (2016) Roles of Nanofiber Scaffold Structure and Chemistry in Directing Human Bone Marrow Stromal Cell Response. Adv Tissue EngRegen Med Open Access 1(1): 00003. DOI: 10.15406/atroa.2016.01.00003